Disparate Exciton-Phonon Couplings for Zone-Center and Boundary Phonons in Solid-State Graphite

Xuefei Feng,[1,†] Shawn Sallis,[1,†] Yu-Cheng Shao,[1,2] Ruimin Qiao,[1] Yi-Sheng Liu,[1] Li Cheng Kao,[1] Anton S. Tremsin,[3] Zahid Hussain,[4] Wanli Yang,[1] Jinghua Guo,[1] and Yi-De Chuang[1,*]

[1]*Advanced Light Source, Lawrence Berkeley National Laboratory, Berkeley, California 94720, USA*
[2]*Department of Physics, University of Houston, Houston, Texas 77204, USA*
[3]*Space Science Laboratory, University of California, Berkeley, California 94720, USA*
[4]*Materials Science Division, Lawrence Berkeley National Laboratory, Berkeley, California 94720, USA*

(Received 28 January 2020; revised 26 April 2020; accepted 28 July 2020; published 8 September 2020)

The exciton-phonon coupling in highly oriented pyrolytic graphite is studied using resonant inelastic x-ray scattering (RIXS) spectroscopy. With ~70 meV energy resolution, multiple low energy excitations associated with coupling to phonons can be clearly resolved in the RIXS spectra. Using resonance dependence and the closed form for RIXS cross section without considering the intermediate state mixing of phonon modes, the dimensionless coupling constant g is determined to be 5 and 0.35, corresponding to the coupling strength of 0.42 eV $+/-$ 20 meV and 0.20 eV $+/-$ 20 meV, for zone center and boundary phonons, respectively. The reduced g value for the zone-boundary phonon may be related to its double resonance nature.

DOI: 10.1103/PhysRevLett.125.116401

Carbon based materials, such as graphite, graphene, diamond, fullerene, and carbon nanotubes, have attracted much attention due to their unique electric and thermal properties that can be used in the next generation electronic devices [1–3]. However, the lack of detailed understanding on the nature of interactions in these materials limits the ability to establish the relationship between their electronic structures and the prospective device performance. For example, the electron-phonon coupling (EPC), which determines material properties like thermal and electric conductivities, is one of the most important interactions in condensed matter systems [4]. The EPC also plays a critical role in the emergent phenomena like high T_C superconductivity and its competing density wave states [5–9]. Although various techniques have been used to study the EPC-related phenomena in carbon based materials, it's still challenging to determine the key parameter like the coupling constant experimentally [10–24].

Resonant inelastic x-ray scattering (RIXS) spectroscopy has recently been shown as a promising technique for studying the EPC in correlated materials [25–32]. In the RIXS process, the presence of core hole will change the local configuration around the interaction site [33–37]. When the photoexcited electron interacts with lattice vibrations during its decay to fill in the core hole, as illustrated in the Frank-Condon picture in Fig. 1(a), the EPC can be investigated through the induced energy loss features in the RIXS spectra [38,39]. Complementary to other techniques, RIXS is sensitive to the chemical, orbital, and bonding states of probed element and access the momentum-resolved EPC [40,41]; in addition, the core-hole lifetime can be reduced by detuning the excitation photon energy away from resonance [37], effectively changing the probing timescale.

Clear phonon overtones in the RIXS spectra have been seen mainly in the molecular systems, whose finite size further permits the detailed analysis on the energy landscape and Rydberg levels for explaining these overtones [42–47]. However, such an approach becomes a daunting task if not impossible for correlated materials. In fact, clear phonon excitations are rarely seen in the RIXS spectra of correlated materials except for the ones with strong EPC [25,27,31]. In that regard, the current RIXS studies on highly oriented pyrolytic graphite (HOPG) can serve as a pedagogical example between these two limits.

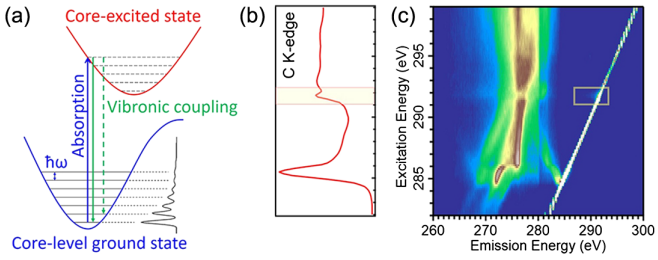

FIG. 1. (a) Schematic illustration of the Frank-Condon picture showing the transition from vibrationally excited states to the ground state. (b) Total electron yield mode of the XAS spectrum at the C K edge recorded with sample surface normal at 55° angle at room temperature. (c) RIXS map of HOPG at room temperature. The broadening of the elastic peak is observed at excitation energies between 291 eV and 292 eV (light yellow box). Reprinted from Ref. [50] with the permission of AIP Publishing.

Despite a long history that can be traced back to the 1990s, RIXS studies on the EPC of carbon based materials have been limited by the poor energy resolution around 0.2 eV at the C K edge, which is too coarse to resolve the phonon excitations [48,49]. Here we revisit this topic with an improved energy resolution that enables us to clearly resolve multiple phonon excitations. The x-ray absorption (XAS) and RIXS experiments were carried out on the *ex situ* cleaved, commercial HOPG at both iRIXS and qRIXS end stations at beam line 8.0.1 at the Advanced Light Source (ALS), Lawrence Berkeley National Laboratory (LBNL) [50–53]. The experimental geometry is shown in Fig. 3(a) and details can be found in the Supplemental [54].

The C K edge XAS spectrum shown in Fig. 1(b) was collected in the total electron yield (TEY) mode with the sample surface normal at 55° relative to the incident x-ray beam. The sharp features at 285.4 and 291.8 eV can be assigned to the excitations to the unoccupied π^* and σ^* states, respectively (see Supplemental [54]) [33,48,58]. The RIXS map recorded at the same geometry with the x-ray spectrometer placed at 90° scattering angle is shown in Fig. 1(c). The dominant features with emission energies between 270 and 280 eV are from the band transitions [33,34]. Zooming in the elastic peak region (zero energy loss, the white diagonal line), one can see broadening when the excitation photon energies are tuned to C $1s \rightarrow \pi^*$ and σ^* resonances. The strong dispersive shoulder next to the elastic peak around π^* resonance can be attributed to the transition from the occupied σ band at the Γ point to the C $1s$ core level, whose dispersion is manifested by the energy and momentum conservation with respect to the band structure. On the other hand, the broadening around σ^* resonance (yellow box) is related to the presence of phonon excitations that is the main focus of this work [48].

With an improved energy resolution down to ~70 meV and a proper arrangement of sample and spectrometer angles (values listed in each figure) to optimize the relative intensity between the elastic peak and low energy excitations, the resulting photon energy-dependent RIXS spectra at room temperature are shown in Fig. 2(a) [53]. From these spectra, one sees that a small hump around 200 meV energy loss (pink curve) becomes a dominant feature when the excitation photon energy is tuned to the σ^* resonance (black curve). In the meantime, multiple broad humps up to ~1 eV energy loss gain the intensity and are clearly resolved in the spectra. These features, *tentatively* regarded as the overtones of the fundamental at ~200 meV energy loss, may be explained by the Frank-Condon xpicture in Fig. 1(a). The decrease in their intensities with increasing the detuning Ω [$= \hbar(\omega_{\text{in}} - \omega_{\text{res}})$] from resonance ($\hbar\omega_{\text{res}}$) can also be understood as when the core-hole lifetime becomes much shorter, the RIXS channel that involves slower degrees of freedom, like lattice, can be suppressed [37].

For quantitative analysis, we fit these low energy excitations in the 298 K, 291.8 eV spectrum [markers, Fig. 2(b)] with Voigt functions (thin lines). The obtained peak energy position and the full width at half maximum (FWHM) are summarized in Figs. 2(c) and 2(e), respectively. Although the peak position versus peak number seems to display a linear relationship, a close inspection shows that there are subtle variations. The positions of peak No. 2 to No. 6 consistently deviate from the linear extrapolation between the elastic peak (No. 0) and first peak (No. 1), and the deviation exceeds the blue shaded region that denotes the possible peak energies when taking the error bar of peak No. 1 into consideration. The subtlety becomes evident if plotting the energy difference between the adjacent peaks [see Fig. 2(d)]: the clear oscillatory behavior is too large to be accounted for by the fitting errors. This variation implies that the energy of peak No. n ($n =$ integer) is not the multiple of the first peak at 190 ± 7 meV; instead, it is shifted towards lower energy loss with nonuniform offset. In addition, the FWHM of peak No. 2 is larger compared with the first and even the third peak, and the magnitude cannot be explained by the fitting error either.

We repeated the measurement at 80 K [bottom panel in Fig. 2(b)] and the fitting results are shown as red open circles in Figs. 2(c)–2(f). Besides the enhanced elastic peak at 80 K due to the transferred spectral weight from phonon excitations, the intensity ratio between the first and the other peaks, as well as the peak energy position, are all temperature independent [even displayed in the energy difference plot in Fig. 2(c)]. The only discrepancy we can see is the FWHM of peak No. 2, which is slightly narrower at 80 K. The agreement between the 298 and 80 K data indicates that the observed anomalies in Figs. 2(c)–2(e) are intrinsic. We also vary the sample and spectrometer angles slightly to see how these phonon excitations change with experimental geometry [Fig. 3(a)]. Besides the strong response in the elastic peak [Figs. 3(b)–3(d)], subtle variations can only be seen after fitting these excitations with Voigt functions (colored lines). From the fittings, we conclude that the peak energy positions do not depend on the experimental geometry within the fitting error [Fig. 3(e)], although the relative peak intensities exhibit a weak geometry dependence. We also varied the sample azimuthal angle and the relative intensity between peak No. 1 and No. 2 exhibits a noticeable change (data not shown).

Assuming one active Einstein phonon and the Holstein Hamiltonian, the RIXS cross section can be calculated analytically to yield a closed form [35,36,59]:

$$I_{\text{ph}} \propto \sum_{n'=0}^{\infty} \left| \sum_{n=0}^{n'} \frac{B_{n'n}(g) B_{n0}(g)}{\Omega + i\Gamma + (g-n)\omega_0} + \sum_{n=n'+1}^{\infty} \frac{B_{nn'}(g) B_{n0}(g)}{\Omega + i\Gamma + (g-n)\omega_0} \right|^2 \delta(\omega - n'\omega_0). \quad (1)$$

In this equation, 0, n, and n' are the ground, intermediate, and final state phonon occupation number; g is the

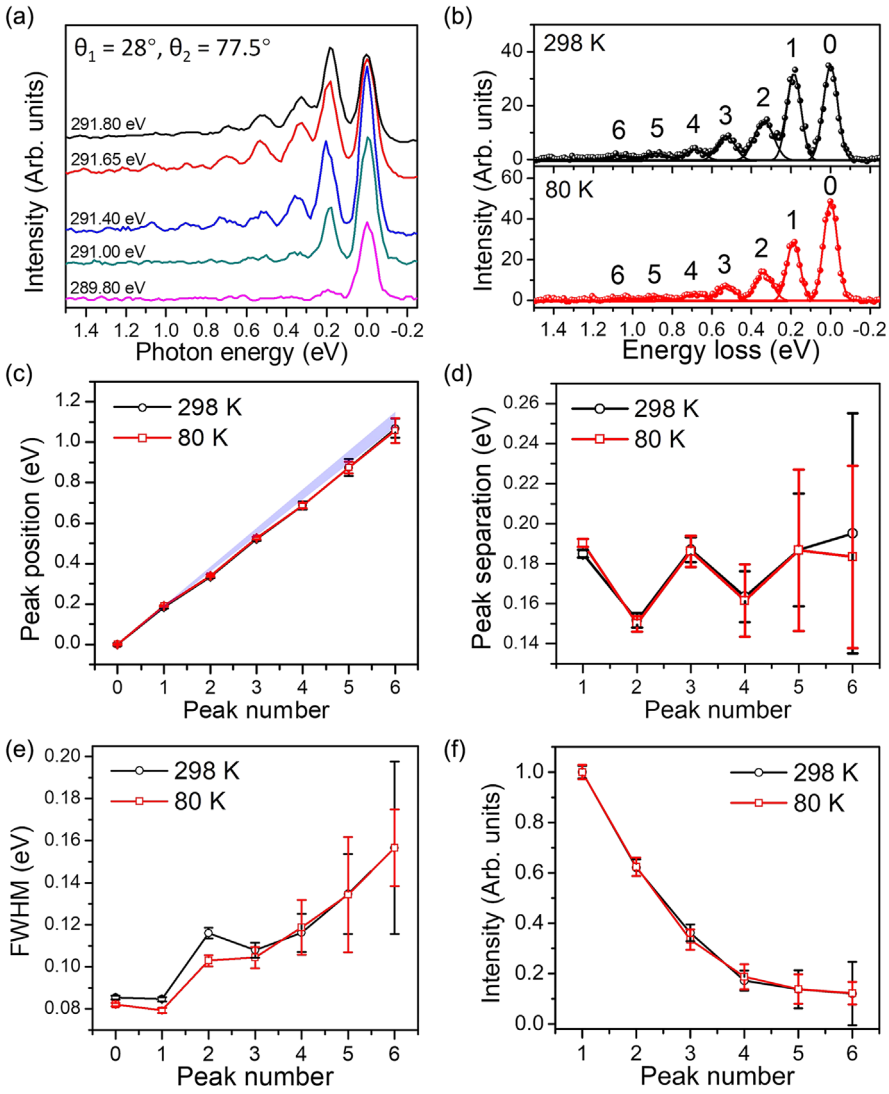

FIG. 2. (a) Room temperature RIXS spectra recorded with excitation energies around the σ^* resonance (291.80 eV). The definition of sample and spectrometer angles are shown in Fig. 3(a). (b) RIXS spectra recorded at 298 (top, black markers) and 80 K (bottom, red markers) with the geometry listed in Fig. 2(a). The excitation photon energy is 291.80 eV. The lines are the Voigt function fitting. The elastic peak and phonons are labeled as peak No. 0 and peaks No. 1–No. 6, respectively. (c) Energy position of the peaks with the elastic peak set to 0 eV. The blue shaded area shows the possible energy position by connecting the peak No. 0 to the maximum and minimum of peak No. 1 (the error bar). (d) The energy difference between the adjacent peaks from panel (c). (e) FWHM of the peaks from the fitting shown in panel (b). (f) Comparison of the intensities of peaks at 80 (red) and 298 K (black). The intensity of peak No. 1 is set to 1.0.

dimensionless EPC; Γ is the inverse core-hole lifetime; ω_0 is the phonon mode energy; and Ω is the detuning of excitation photon energy from resonance. $B_{ab}(g)$ is the Frank-Condon factor. This equation has been used by the RIXS community to calculate the g value in correlated materials by comparing the intensities of phonon overtones (needs minimum the first and the second order peaks) in the RIXS spectra at fixed excitation photon energies. However, by following this approach to analyze our data, one inherently assumes that the peaks No. 2 to No. 5 are the real overtones of the first peak with their energy positions at the multiple of 190 ± 7 meV. This assumption does not agree with the anomalies seen in the peak positions [Figs. 2(c) and 2(d)], the FWHM [Fig. 2(e)], and the relative intensity variations in Fig. 3(f). Instead, these results suggest the presence of different phonon modes besides the overtones in the RIXS spectra. In addition, we note that the EPC determined by this approach would be very large and be in disagreement with the analysis using the detuning method [28,32].

Soft x-ray photons typically do not carry large momentum. For 291.80 eV photon and the spectrometer at 77.5° [Fig. 2(a), the angles are defined in Fig. 3(a)], the photon momentum transfer Δq is around 0.23 A^{-1}, which is ~13%

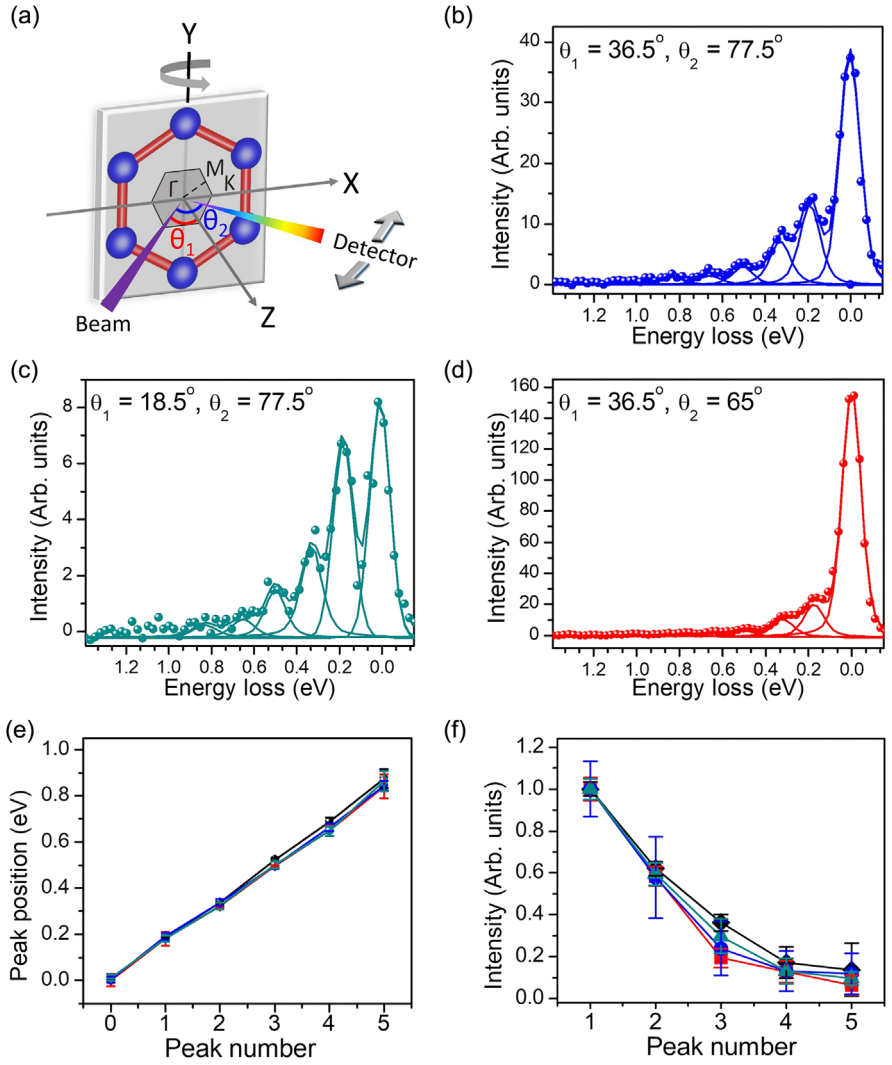

FIG. 3. (a) Schematic diagram of experimental geometry. (b)–(d) Room temperature RIXS spectra with excitation photon energy 291.80 eV and experimental geometry shown in panel (a). The sample and spectrometer angles defined in panel (a) are listed in each figure. (e) The peak energy positions from fitting the spectra in panels (b)–(d) with Voigt functions. (f) The normalized intensities of the peaks from the fitting. The intensity of the first peak is set to 1.0. The symbol color scheme in panels (e) and (f) adopts the trace color scheme in panels (b)–(d). The black symbols in (e) and (f) are from Figs. 2(c) and 2(f) as the reference.

of the Brillouin zone size along the Γ-K direction. At nearly specular geometry, the in-plane projection $\Delta q_{//}$ can be even smaller: only <3% of the Γ-K zone size. Because of this, the conservation of momentum requires the electron coupling to phonon mode(s) with very small net momentum. When the excitation photon energy is tuned to the resonance of σ^* excitonic state, the transition occurs at the bottom of the σ^* band at the Γ point [34]. Since we are effectively looking at the "optical transition" at C $1s \rightarrow \sigma^*$ resonance, we can resort to the results from optical Raman spectroscopy to identify the phonon modes seen in the RIXS spectra [60].

In the optical Raman spectroscopy, there are two prominent phonon modes with E_{2g} (G mode at the Γ point, 1580 cm^{-1} or 196 meV) and A_1 symmetry (D mode at the K point; it becomes Raman active through the double resonance so that its energy is 2700 cm^{-1} or 335 meV), respectively [61]. The energy of these modes agrees very well with the energy position of peak No. 1 and No. 2: peak No. 1 at 190 ± 7 meV can be assigned to the G mode whereas peak No. 2 at 335 ± 7 meV can be assigned to the $2D$ mode. Interestingly, the oscillatory behavior in Fig. 2(d) suggests that the energy of peak No. 3 will be ~190 meV higher than peak No. 2, prompting us to assign it to the $G + 2D$ mode which is also seen in the Raman spectroscopy. The assignment of prominent energy loss features in Fig. 2(b) to different phonon modes, together with the enhanced peaks No. 2 ($2D$) and No. 3 ($G + 2D$) that

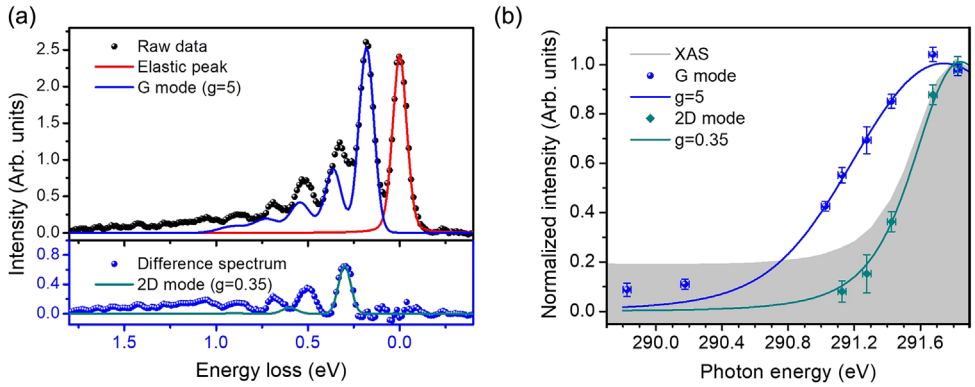

FIG. 4. (a) Top: overlay of experimental (markers) and simulated RIXS spectra for the G mode with $g = 5$ (blue curve; sum of fundamental up to 5th order; for details, see Ref. [54]). The red curve is the fitted elastic peak. Bottom: difference between the experimental spectrum and the sum of the G mode contribution and the elastic peak. The green line shows the simulated $2D$ mode with $g = 0.35$. (b) Overlay of normalized XAS spectrum (shaded area), E_{2g} (G mode) peak intensity (filled blue circles), $2 * A_{1g}$ ($2D$ mode) peak intensity (filled green squares) and the least square fitted curves using Eq. (2). The parameters $\omega_0 = 0.190$ eV for the G mode, $\omega_0 = 0.335$ eV for the $2D$ mode, and $\Gamma = 0.414$ eV (~10 fs) are used in the equation [63]. The justification for the normalization of the G mode intensity is discussed in the Supplemental Material [54].

preclude the separation of overtones like $2G$ and $3G$ from them, prohibit us from using Eq. (1) to fit the intensities of fundamental and high order overtones to extract the g value [27,29–31]. Alternatively, one can use the resonance effect to determine the EPC as recently demonstrated by Rossi *et al.* and Braicovich *et al.*[28,32]. However, the mixing of G and D modes in the virtual intermediate state in the RIXS process can complicate such analysis and lead to a sizable uncertainty in g [62]. Despite lacking the detailed theoretical calculations to account for this intermediate state mixing effect and the knowledge of ground state and intermediate state energy landscapes, following the treatment by Rossi *et al.* and attributing the peak No. 1 solely to the G mode from the longitudinal and transverse optical branches may still yield valuable insight to the nature of the excitonic coupling to these phonons and inspire further theoretical studies [62].

To proceed with this approach, the self-absorption effect is corrected (see the Supplemental Material [54]). The intensity of the G mode obtained from a Voigt function fitting is shown as the blue circles in Fig. 4(b). In the same figure, we also overlay the XAS spectrum (gray shaded area). Unlike in the case of cuprates, the intensity of this phonon remains appreciable even when the excitation photon energy is detuned by ~0.8 eV, suggesting a strong coupling nature. The intensity for exciting a single phonon can be expressed as ($n' = 1$):

$$I_{\mathrm{ph}} \propto \frac{e^{-2g}}{g}\left|\sum_{n=0}^{\infty}\frac{g^n(n-g)}{n![\Omega + i\Gamma + (g-n)\omega_0]}\right|^2. \qquad (2)$$

We use this equation and the least square fitting on the data to obtain a g value of $5 + / - 0.5$ (blue curves). With this g value, the corresponding EPC strength $M_G = \sqrt{g}\omega_0$ is ~0.42 eV $+ / -$ 20 meV.

Assuming the g value does not change with excitation photon energy, we can then calculate its contribution up to 5th order overtone using Eq. (1) ($n' = 1 \sim 5$). For each order, we also linearly broadening (15%) its width as suggested by Fig. 2(e). The sum of these phonon overtones is shown as a blue curve in Fig. 4(a). The G mode contribution and the elastic peak (red curve) are then subtracted from the RIXS spectra (markers) to yield the fundamental of $2D$ mode, see the bottom panel of Fig. 4(a). The intensity of this $2D$ mode is shown as green squares in Fig. 4(b). Contrasting to the behavior of the G mode, the $2D$ mode intensity is quickly suppressed with the increased detuning Ω, indicating a weaker coupling. By performing the same least squares fitting, we obtain a g value of $0.35 + / - 0.07$ which gives the EPC strength M_{2D} of ~0.20 eV $+ / -$ 20 meV.

In the RIXS process, the photoexcited electron and the poorly screened core hole in the form of exciton at the σ^* resonance can exert a much larger perturbation to the surrounding C atoms than the particle-hole pair created in the optical Raman process. With such a large perturbation, phonons like the G and D modes, due to their unique phonon band structure at the Γ and K points that exhibit Kohn anomaly, are the prime candidates to be excited [64–66]. Interestingly, even in the presence of exciton, the ratios of $2D$ and $G + 2D$ modes relative to the G mode obtained from RIXS (relative intensity of 0.22 and 0.12, respectively) are comparable to that of the Raman spectroscopy (0.27 and 0.02) [60]. We note that according to Geondzhian and Gilmore, who presented the RIXS theory involving more than one active phonon mode with the exciton [62], the weight of the $G + 2D$ mode can be enhanced due to the intermediate state coupling between phonons that transfers the spectral weight from the weakly coupled $2D$ mode [see Fig. 4(a)]. We also notice that the

obtained $(M_{2D})^2$ seems to be in agreement with the $g^2_{A'_1}$ from recent time-resolved ARPES (TR-ARPES) despite the fact that these two techniques probe different aspects of phonon coupling of this D mode [22]. However, without considering the intermediate state phonon mixing effect, the fitted coupling strengths M_G and M_{2D} may be overestimated relative to the actual values [62]. Since this $2D$ mode involves double resonance to become Raman active (also for RIXS), we conjecture that the scattering cross section will be suppressed once core-hole lifetime is reduced, resulting in a smaller coupling constant compared to that of the G mode. Amid the extensive spectroscopic studies over the past decades to understand the phonons in HOPG and their couplings to electrons or excitons, our work demonstrates that active phonons in HOPG can couple differently to the exciton and certain techniques may preferentially enhance the respective coupling strengths [22,60]. The exciton-phonon coupling obtained from RIXS is in contrast to the electron-phonon couplings from other spectroscopies and how these coupling constants are related to the transport properties of HOPG remains to be elucidated by further theoretical studies; nevertheless, our RIXS study offers a different insight to the phonon dynamics in the presence of strong photon-induced exciton, which is an interesting research topic in the photophysics of carbon materials [67]. The improved RIXS spectral resolution coupled to versatile tuning knobs like resonance, experimental geometry, etc., can facilitate the determination and differentiation of phonon excitations in carbon-based materials, shedding light on the nature of phononic interactions that can be useful for carbon-based energy applications [68,69].

We thank K. Gilmore, M. X. Na, A. Damascelli, and A. F. Kemper for the insightful discussion. This research used resources of the Advanced Light Source, a U.S. DOE Office of Science User Facility under Contract No. DE-AC02-05CH11231. The Timepix detector activity is supported by FWP #RoyTimepixDetector. X. F. acknowledges the support of the Joint Center for Energy Storage Research (JCESR), an Energy Innovation Hub funded by the U.S. DOE, office of Science, Basic Energy Sciences.

*To whom all correspondence should be addressed.
ychuang@lbl.gov
†These authors contributed equally to this work.

[1] D. D. L. Chung, *Carbon Materials: Science and Applications* (World Scientific, New York, USA, 2019).
[2] S. Choi, S. I. Han, D. Kim, T. Hyeon, and D. H. Kim, Chem. Soc. Rev. **48**, 1566 (2019).
[3] A. A. Balandin, Nat. Mater. **10**, 569 (2011).
[4] C. Kittel, *Introduction to Solid State Physics* (John Wiley & Sons, Inc., Hoboken, 2004).
[5] J. J. Lee *et al.*, Nature (London) **515**, 245 (2014).
[6] L. Chaix *et al.*, Nat. Phys. **13**, 952 (2017).
[7] D. Reznik, L. Pintschovius, M. Ito, S. Iikubo, M. Sato, H. Goka, M. Fujita, K. Yamada, G. D. Gu, and J. M. Tranquada, Nature (London) **440**, 1170 (2006).
[8] A. Lanzara *et al.*, Nature (London) **412**, 510 (2001).
[9] S. Gerber *et al.*, Science **357**, 71 (2017).
[10] P. J. Benning, J. L. Martins, J. H. Weaver, L. P. F. Chibante, and R. E. Smalley, Science **252**, 1417 (1991).
[11] C. Faugeras, M. Amado, P. Kossacki, M. Orlita, M. Sprinkle, C. Berger, W. A. de Heer, and M. Potemski, Phys. Rev. Lett. **103**, 186803 (2009).
[12] A. P. Shreve, E. H. Haroz, S. M. Bachilo, R. B. Weisman, S. Tretiak, S. Kilina, and S. K. Doorn, Phys. Rev. Lett. **98**, 037405 (2007).
[13] L. Lüer, C. Gadermaier, J. Crochet, T. Hertel, D. Brida, and G. Lanzani, Phys. Rev. Lett. **102**, 127401 (2009).
[14] A. W. Bushmaker, V. V. Deshpande, M. W. Bockrath, and S. B. Cronin, Nano Lett. **7**, 3618 (2007).
[15] J. Yan, Y. B. Zhang, P. Kim, and A. Pinczuk, Phys. Rev. Lett. **98**, 166802 (2007).
[16] Y. Yin, A. N. Vamivakas, A. G. Walsh, S. B. Cronin, M. S. Ünlü, B. B. Goldberg, and A. K. Swan, Phys. Rev. Lett. **98**, 037404 (2007).
[17] A. Gambetta *et al.*, Nat. Phys. **2**, 515 (2006).
[18] S. Sapmaz, P. Jarillo-Herrero, Y. M. Blanter, C. Dekker, and H. S. J. van der Zant, Phys. Rev. Lett. **96**, 026801 (2006).
[19] K. Ienaga *et al.*, Nano Lett. **17**, 3527 (2017).
[20] A. Bhaumik, R. Sachan, S. Gupta, and J. Narayan, ACS Nano **11**, 11915 (2017).
[21] K. Sugawara, T. Sato, S. Souma, T. Takahashi, and H. Suematsu, Phys. Rev. Lett. **98**, 036801 (2007).
[22] M. X. Na *et al.*, Science **366**, 1231 (2019).
[23] A. C. Ferrari *et al.*, Phys. Rev. Lett. **97**, 187401 (2006).
[24] S.-i. Tanaka, K. Mukai, and J. Yoshinobu, Phys. Rev. B **95**, 165408 (2017).
[25] D. Meyers, K. Nakatsukasa, S. Mu, L. Hao, J. Yang *et al.*, Phys. Rev. Lett. **121**, 236802 (2018).
[26] V. Ilakovac, S. Carniato, P. Foury-Leylekian, S. Tomić, J.-P. Pouget, P. Lazić, Y. Joly, K. Miyagawa, K. Kanoda, and A. Nicolaou, Phys. Rev. B **96**, 184303 (2017).
[27] S. Fatale, S. Moser, J. Miyawaki, Y. Harada, and M. Grioni, Phys. Rev. B **94**, 195131 (2016).
[28] M. Rossi *et al.*, Phys. Rev. Lett. **123**, 027001 (2019).
[29] W. S. Lee *et al.*, Phys. Rev. Lett. **110**, 265502 (2013).
[30] S. Moser, S. Fatale, P. Krüger, H. Berger, P. Bugnon, A. Magrez, H. Niwa, J. Miyawaki, Y. Harada, and M. Grioni, Phys. Rev. Lett. **115**, 096404 (2015).
[31] J. G. Vale *et al.*, Phys. Rev. B **100**, 224303 (2019).
[32] L. Braicovich *et al.*, arXiv:1906.01270.
[33] M. van Veenendaal and P. Carra, Phys. Rev. Lett. **78**, 2839 (1997).
[34] J. A. Carlisle, E. L. Shirley, E. A. Hudson, L. J. Terminello, T. A. Callcott, J. J. Jia, D. L. Ederer, R. C. Perera, and F. J. Himpsel, Phys. Rev. Lett. **74**, 1234 (1995).
[35] L. Ament, https://openaccess.leidenuniv.nl/bitstream/handle/1887/16138/proefschrift-ament-final.pdf?sequence=2 (2010).
[36] L. J. P. Ament, M. van Veenendaal, T. P. Devereaux, J. P. Hill, and J. van den Brink, Rev. Mod. Phys. **83**, 705 (2011).
[37] F. Gel'mukhanov and H. Ågren, Phys. Rep. **312**, 87 (1999).
[38] E. Condon, Phys. Rev. **28**, 1182 (1926).

[39] J. Franck, Trans. Faraday Soc. **21**, 536 (1926).
[40] A. Geondzhian and K. Gilmore, Phys. Rev. B **98**, 214305 (2018).
[41] T. P. Devereaux *et al.*, Phys. Rev. X **6**, 041019 (2016).
[42] F. Hennies, A. Pietzsch, M. Berglund, A. Föhlisch, T. Schmitt, V. Strocov, H. O. Karlsson, J. Andersson, and J.-E. Rubensson, Phys. Rev. Lett. **104**, 193002 (2010).
[43] Y. Harada *et al.*, Phys. Rev. Lett. **111**, 193001 (2013).
[44] S. Schreck *et al.*, Sci. Rep. **6**, 20054 (2016).
[45] J.-E. Rubensson *et al.*, Phys. Rev. Lett. **114**, 133001 (2015).
[46] R. C. Couto *et al.*, Nat. Commun. **8**, 14165 (2017).
[47] V. Vaz da Cruz *et al.*, Nat. Commun. **10**, 1013 (2019).
[48] Y. Ma, P. Skytt, N. Wassdahl, P. Glans, D. C. Mancini, J. Guo, and J. Nordgren, Phys. Rev. Lett. **71**, 3725 (1993).
[49] L. Zhang, X. Li, A. Augustsson, C. M. Lee, J.-E. Rubensson, J. Nordgren, P. N. Ross, and J. H. Guo, Appl. Phys. Lett. **110**, 104106 (2017).
[50] R. Qiao *et al.*, Rev. Sci. Instrum. **88**, 033106 (2017).
[51] Y.-D. Chuang *et al.*, Rev. Sci. Instrum. **88**, 013110 (2017).
[52] N. C. Andresen, P. Denes, A. Goldschmidt, J. Joseph, A. Karcher, and C. S. Tindall, Rev. Sci. Instrum. **88**, 083103 (2017).
[53] Y.-D. Chuang *et al.*, J. Electron Spectrosc. Relat. Phenom. https://doi.org/10.1016/j.elspec.2019.146897 (2019).
[54] See Supplemental Material at http://link.aps.org/supplemental/10.1103/PhysRevLett.125.116401 for experimental details, Self-Absorption Correction for RIXS spectra, background treatment of XAS spectra, and the estimate of EPCs, which includes Refs. [55–57].
[55] M. Minola, G. Dellea, H. Gretarsson, Y. Y. Peng, Y. Lu *et al.*, Phys. Rev. Lett. **114**, 217003 (2015).
[56] R. Fumagalli, L. Braicovich, M. Minola, Y. Y. Peng, K. Kummer *et al.*, Phys. Rev. B **99**, 134517 (2019).
[57] S. Eisebitt, T. Böske, J.-E. Rubensson, and W. Eberhardt, Phys. Rev. B **47**, 14103 (1993).
[58] O. Wessely, M. I. Katsnelson, and O. Eriksson, Phys. Rev. Lett. **94**, 167401 (2005).
[59] L. J. P. Ament, M. van Veenendaal, and J. van den Brink, Eur. Phys. Lett. **95**, 27008 (2011).
[60] Y. Kawashima and G. Katagiri, Phys. Rev. B **52**, 10053 (1995).
[61] C. Thomsen and S. Reich, Phys. Rev. Lett. **85**, 5214 (2000).
[62] A. Geondzhian and K. Gilmore, Phys. Rev. B **101**, 214307 (2020).
[63] Y. Harada, T. Tokushima, Y. Takata, T. Takeuchi, Y. Kitajima, S. Tanaka, Y. Kayanuma, and S. Shin, Phys. Rev. Lett. **93**, 017401 (2004).
[64] R. P. Chatelain, V. R. Morrison, B. L. M. Klarenaar, and B. J. Siwick, Phys. Rev. Lett. **113**, 235502 (2014).
[65] H. Yan, D. Song, K. F. Mak, I. Chatzakis, J. Maultzsch, and T. F. Heinz, Phys. Rev. B **80**, 121403 (2009).
[66] S. Piscanec, M. Lazzeri, F. Mauri, A. C. Ferrari, and J. Robertson, Phys. Rev. Lett. **93**, 185503 (2004).
[67] M. S. Dresselhaus, G. Dresselhaus, R. Saito, and A. Jorio, Annu. Rev. Phys. Chem. **58**, 719 (2007).
[68] S. Ren, D. Joulié, D. Salvatore, K. Torbensen, M. Wang, M. Robert, and C. P. Berlinguette, Science **365**, 367 (2019).
[69] F. Li *et al.*, Nature (London) **577**, 509 (2020).